

Selection constraints on high redshift quasar searches in the VISTA kilo-degree infrared galaxy survey

J. R. Findlay,^{1*} W. J. Sutherland,¹ B. P. Venemans,² C. Reylé,³ A. C. Robin,⁴
D. G. Bonfield,⁴ V. A. Bruce⁵ and M. J. Jarvis.^{4,6}

¹*Astronomy Unit, Queen Mary, University of London, London E1 4NS.*

²*European Southern Observatory, Karl-Schwarzschild-Strasse 2, 85748 Garching bei Munchen, Germany.*

³*Université de Franche-Comté, Institut UTINAM, UMR CNRS 6213, Observatoire des Sciences de l'Univers THETA de Franche-Comté, Observatoire de Besançon, BP 1615, 25010 Besançon Cedex, France.*

⁴*Centre for Astrophysics, Science & Technology Research Institute, University of Hertfordshire, Hatfield, Herts, AL10 9AB, UK.*

⁵*SUPA Institute for Astronomy, University of Edinburgh, Royal Observatory, Edinburgh EH9 3HJ*

⁶*Physics Department, University of the Western Cape, Cape Town, 7535, South Africa.*

Accepted XXX. Received XXX; in original form XXX

ABSTRACT

The European Southern Observatory’s (ESO) Visible and Infrared Survey Telescope for Astronomy (VISTA) is a 4-m class survey telescope for wide-field near-infrared imaging. VISTA is currently running a suite of six public surveys, which will shortly deliver their first Europe wide public data releases to ESO. The VISTA Kilo-degree Infrared Galaxy Survey (VIKING) forms a natural intermediate between current wide shallow, and deeper more concentrated surveys, by targeting two patches totalling 1500 deg² in the northern and southern hemispheres with measured 5 σ limiting depths of $Z \simeq 22.4$, $Y \simeq 21.4$, $J \simeq 20.9$, $H \simeq 19.9$ and $K_s \simeq 19.3$ (Vega). This architecture forms an ideal working parameter space for the discovery of a significant sample of $6.5 \leq z \leq 7.5$ quasars. In the first data release priority has been placed on small areas encompassing a number of fields well sampled at many wavelengths, thereby optimising science gains and synergy whilst ensuring a timely release of the first products. For rare object searches e.g. high- z quasars, this policy is not ideal since photometric selection strategies generally evolve considerably with the acquisition of data. Without a reasonably representative data set sampling many directions on the sky it is not clear how a rare object search can be conducted in a highly complete and efficient manner.

In this paper, we alleviate this problem by supplementing initial data with a realistic model of the spatial, luminosity and colour distributions of sources known to heavily contaminate photometric quasar selection spaces, namely dwarf stars of spectral type M, L and T. We use this model along with a subset of available data to investigate contamination of quasar selection space by cool stars and galaxies and lay down a set of benchmark selection constraints that limit contamination to reasonable levels whilst maintaining high completeness as a function of both magnitude and redshift. We review recent follow-up imaging of the first VIKING high- z quasar candidates and find that the results lend considerable support for the choice of selection constraints. The methods outlined here are also applicable to rare object searches in a number of other ongoing and forthcoming projects.

Key words: surveys - techniques: photometric - galaxies: high-redshift - quasars: general

1 INTRODUCTION

The existence of luminous quasars at $z \sim 6^1$ suggests that the formation of the first supermassive black holes began

* E-mail: j.findlay@qmul.ac.uk

¹ There are a number of variables which are conventionally denoted z or Z . To avoid confusion they are defined here as z ; redshift, z ; the SDSS passband, Z ; the VISTA passband.

within the first few hundred million years of the big bang. As such high- z quasars offer powerful probes of the early Universe, setting constraints on early structure formation (Stiavelli et al. 2005; Willott et al. 2005a; Shen et al. 2007, etc.), chemical enrichment (Maiolino 2009, and refs. therein) and the state of the inter-galactic medium at the end of cosmic re-ionisation (Fan et al. 2006).

In the last decade, optical surveys such as the Sloan Digital Sky Survey (SDSS; York et al. 2000) and the Canada France High- z Quasar Survey (CFHQS; Willott et al. 2005b) have increased the number of known quasars at $z \sim 6$ to over 50 (e.g. Jiang et al. 2008; Willott et al. 2010). At the single scan sensitivity limit of the Sloan camera ($z \simeq 21.0$) the surface density of $z \geq 6$ quasars brighter than $z \leq 21$ is of order $\rho_Q \simeq 0.01 \text{ deg}^{-2}$, so this represents a considerable effort.

High- z quasars are generally initially selected for follow-up observations by virtue of their photometric colours. The key to the photometric detection of a strong quasar candidate is to isolate the characteristic flux break blueward of the Lyman-alpha ($\text{Ly-}\alpha$) transition brought about by the thickening of the $\text{Ly-}\alpha$ forest towards higher redshifts. Colour selection techniques exploit this break by placing a blue observing band across the $\text{Ly-}\alpha$ transition and a further band just redward. Objects suitable for follow-up spectroscopy should then present themselves as extremely red faint point sources. A carefully placed colour cut is usually sufficient to confine the most interesting sources to a region of colour space distinct from most main sequence stars and galaxies. In principle, this facilitates candidate selection in just two passbands, but in practice a third passband is necessary to permit a measurement of the continuum level redward of $\text{Ly-}\alpha$ as a means of reducing contamination from cool degenerate stars. This is the technique pioneered by the SDSS and adopted in the CFHQS; both make initial selections in $i - z$ and take follow-up J-band imaging of promising candidates prior to spectroscopic confirmation (Fan et al. 2001; Willott et al. 2005b).

At $z > 6$ $\text{Ly-}\alpha$ begins to shift out of the Sloan z band and while projects like the Panoramic Survey Telescope and Rapid Response System (Pan-STARRS; Kaiser et al. 2002) aim to progress towards higher redshifts in a predominantly optical parameter space (by selecting i dropouts), faint optical detections make it difficult to reject the numerous Galactic stars with scattered quasar-like colours that can outnumber high- z quasars by a factor 10^4 .

To this end a number of other surveys have taken a different approach, employing the near-IR as their selection space, a tactic which has had recent encouraging success in the UKIRT Infrared Deep Sky Survey (UKIDSS; Lawrence et al. 2007). One of the innovations behind the UKIDSS photometric system, was to recognise that near-IR filter combinations incorporating z , J, H and K alone are inadequate for $z > 6$ quasar selection, since cool star spectra tend to peak in the near-IR and crowd the quasar colour-colour locus (Warren & Hewett 2002). The solution was to introduce an observing band intermediate between z and J and was put forward by Hewett et al. (2006). The Y-band filter was optimised for this purpose and has been used to great effect in the UKIDSS-LAS (UKIDSS Large Area Survey; Lawrence et al. 2007) where seven $z \gtrsim 6$ quasars have been identified up to the UKIDSS eighth data release

(Venemans et al. 2007; Mortlock et al. 2009; Mortlock et al. 2011, Venemans et. al. in preparation, Patel et al. in preparation).

Working in the same parameter space as UKIDSS is the European Southern Observatory's (ESO) Visible and Infrared Survey Telescope for Astronomy (VISTA), a 4-m class wide field survey telescope located at ESO's Paranal observatory in Chile (Emerson & Sutherland 2010). More than 80 per cent of VISTA time is devoted to running a suite of six public surveys, which will deliver European public data releases in the near future. Of these projects, the VISTA Kilo-degree Infrared Galaxy survey (VIKING) has a combination of depth and area that is ideally suited for quasar searches at the highest redshifts. Over the nominal five year survey life span, VIKING will image a total of 1500 deg^2 in the Z, Y, J, H, Ks near-IR bandpasses centred on the northern Galactic cap and the southern Galactic pole. VIKING will detect in excess of 6×10^6 stars and 20×10^6 galaxies down to a limiting 5σ detection limit of $J \simeq 20.9$ (Vega system).

VISTA's transmission curves are shown in Figure 1. These include the relevant contributions from the instrument and detector, mirror reflectivity and transmissions through the atmosphere and filters under typical photometric conditions. Also plotted is the Large Bright Quasar Survey's (LBQS; Hewett et al. 1995) template quasar spectrum (Francis et al. 1991), redshifted to $z = 6.8$ and with the characteristic HI absorption trough artificially imposed blueward of redshifted $\text{Ly-}\alpha$ at $\lambda(\text{Ly-}\alpha) = 1216 \text{ \AA} \times 7.8$. The spectra of cool M8- and T5-dwarf stars are plotted alongside the quasar spectrum to highlight, the recognised difficulty of differentiating between high- z quasars and cool stars at the foot of the main sequence and below the hydrogen burning cut-off.

M-dwarfs outnumber high- z quasars by at least a factor $\sim 10^5$ (e.g. Bochanski et al. (2010), obtained a volume limited sample of $\sim 15 \times 10^6$ SDSS objects with M-dwarf like colours at $z < 21.2$. Over a similar depth and area there are currently 19 SDSS quasars with $z \sim 6$ reported by Fan et al. (2006.), while the cooler L and T spectral types are by all accounts, a lot more rare (Lodieu et al. 2009; Burningham et al. 2010). The broad similarities between high- z quasar and M-dwarf spectra, coupled with their relative surface densities means that most colour selected high- z quasar candidates are in fact M-dwarfs with scattered quasar like colours resulting from large photometric errors. The function of a good colour selection criterion then, is to maintain a large selection space while simultaneously minimising contamination from false positives and optimising the completeness of the search.

In the vein of other wide field imaging surveys before it, the initial VIKING data release consists of a few high priority fields to provide a testbed for future larger releases. In the first public VIKING data release $\sim 75 \text{ deg}^2$ will be made available. Precision selection strategies can be developed with a detailed understanding of the error perturbed magnitude and colour distributions of the target and contaminant populations, both as a function of redshift and direction on the sky. These strategies will no doubt develop with the accumulation of large amounts of data. However, the first photometric follow-up of VIKING candidates was undertaken in summer 2011. Although by this time there

was $\sim 350 \text{ deg}^2$ of data available, there was insufficient time to analyse it in detail other than to select candidates based on selection constraints derived from smaller initial data sets. Thus, to optimise selection constraints and provide a complete, efficient and non-biased search it was necessary to use a combination of initial data and detailed modelling (e.g. Fan 1999).

The following article describes a model of the magnitude, colour and spatial distributions of the cool star and quasar populations, which was developed and assessed along with $\sim 200 \text{ deg}^2$ of initial imaging data to lay down some baseline magnitude and colour selection criteria to apply to the $\sim 350 \text{ deg}^2$ available for the first follow-up observations.

The paper is organised as follows; In Section 2 VIKING Vega system synthetic photometry is computed for typical examples of cool-stars and quasars. In Section 3 offsets from the Vega system are measured in the VIKING data. In Section 4 the synthetic photometry is employed along with number count models to populate a synthetic realisation of the cool-star and high- z quasar component of the VIKING catalogue. In Section 5 the catalogue and available data are used to place constraints on quasar selection space and assess completeness. In Section 6 we assess the selection criterion in light of recent followup observations. We summarise our findings and outline future work in Section 7.

Henceforth, all quoted photometry is defined on the Vega system, such that Vega is a zero magnitude star in all VISTA passbands. Magnitudes are quoted in the traditional logarithmic form except for those in the Z band, which are quoted in the asinh form (Lupton et al. 1999). asinh magnitudes take the same values as the equivalent logarithmic form for high signal-to-noise (S/N) measurements, but have the advantage of linear dependence at low S/N or even negative flux, which will be the case for most $z \gtrsim 6.5$ quasars. A softening parameter denoted b , is required to define the scale at which linear dependence dominates. For the Z band we choose b equivalent to $Z = 24.1$, which gives the asinh magnitude of an object with zero flux and is set approximately equal to the sky noise seen in the initial data frames.

Throughout this work we adopt the following values for the Hubble constant and the matter and cosmological constant energy density parameters; $H_0 = 70 \text{ km s}^{-1} \text{ Mpc}^{-1}$, $\Omega_M = 0.28$ and $\Omega_\Lambda = 0.72$ respectively (Komatsu et al. 2009).

2 Z, Y, J SYNTHETIC PHOTOMETRY AND CHARACTERISTIC COLOURS

Characteristic colours were calculated for a set of cool stars and quasars by integrating the product of their spectra and the VISTA response functions², including measured values for the wavelength-dependent losses resulting from atmospheric extinction, mirror reflectivity and instrument and detector response.

² <http://www.eso.org/sci/facilities/paranal/instruments/vista/inst/>

2.1 High-redshift quasars

In order to obtain a representative spread of quasars in colour-colour space, we use a sample of 386 quasars from the SDSS Quasar Catalogue IV (Schneider et al. 2007). The sample spans a redshift range of $3.1 \lesssim z \lesssim 3.2$, over which there is low stellar contamination and high completeness (Richards et al. 2002).

Recent comparisons between high and low- z quasar spectra have shown no obvious evidence for metallicity evolution in the rest-frame UV spectral energy distributions (Jiang et al. 2007; Juarez et al. 2009; Mortlock et al. 2011, although see Jiang et al. 2010 for possible evolution of dust properties). Thus, it is a reasonable approximation to simulate intrinsic quasar spectral energy distributions at $z \geq 6.5$ by artificially redshifting the low- z SDSS sample.

Significant differences between $z \gtrsim 6.5$ quasars and those at lower redshift are apparent blueward of Ly- α due to increasingly strong absorption in the intergalactic medium with redshift. At $z = 6.5$ the optical depth of the intergalactic medium to Ly- α photons is $\gg 1$ (e.g. Fan et al. 2006). For the same neutral density the optical depths to Ly- β and Ly- γ are factors of 6.2 and 17.9 less than for that of Ly- α , but their line strengths are comparatively small and they can be reasonably neglected (e.g. Wiese et al. 1966). Transmission blueward of $\lambda = 1216 \text{ \AA} (1 + z)$ is thus effectively nil, and absorption by intergalactic hydrogen can be adequately modelled in $z \geq 6.5$ quasar spectra by setting transmission shortward of redshifted Ly- α to zero.

2.2 Stars

A library of cool star spectra has been collected from the literature covering VISTA's Z, Y, J, H and K_s passbands, these include all 21 M-, 30 L- and 22 T-dwarf spectra on which Hewett et al. (2006) conducted synthetic photometry in the WFCAM passbands. References for these objects can be found in the above paper. The library is further supplemented by spectra obtained from the DwarfArchives³, the IRTF (NASA Infrared Telescope Facility) spectral library⁴, the SpeX Prism spectral library⁵, the Keck LRIS (Low Resolution Imaging Spectrometer) spectral library⁶ and Sandy Leggett's L- and T-dwarf archives⁷.

2.3 Selection in Z, Y, J

The resulting synthetic colours have been checked for consistency by convolving stellar sources in the WFCAM passbands and comparing results with those presented for the same sources by Hewett et al. (2006) finding good agreement between the two. There is also broad agreement between these results and observational work (e.g. Zhang et al. 2009; Leggett et al. 2010). Simulated $i - z$ colours of the quasar sample over the SDSS passbands are also consistent with the corresponding SDSS photometry.

At this stage it is useful to review the general approach

³ <http://spider.ipac.caltech.edu/staff/davy/ARCHIVE/links.shtml>

⁴ http://irtfweb.ifa.hawaii.edu/~spex/IRTF_Spectral_Library/

⁵ <http://pono.ucsd.edu/~adam/browndwarfs/spexprism/>

⁶ <http://www.stsci.edu/~inr/ultracool.html>

⁷ <http://staff.gemini.edu/~sleggett/LTdata.html>

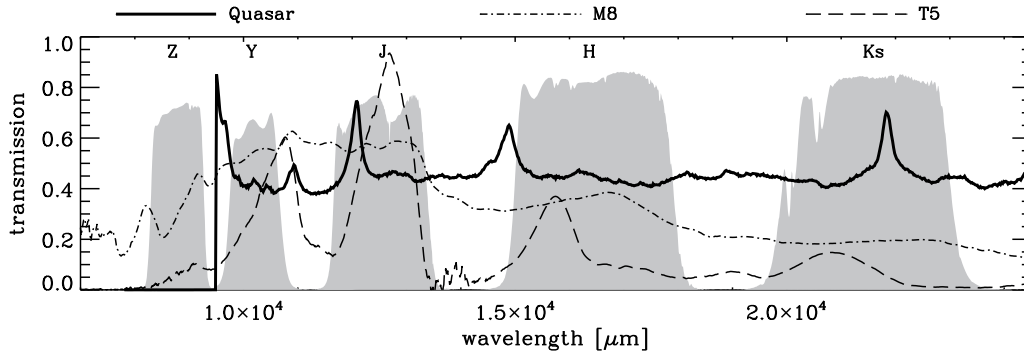


Figure 1. Transmission curves for the VISTA Z, Y, J, H, Ks photometric system, including wavelength dependent losses are labelled and shaded grey. Also shown is the LBQS template quasar spectrum artificially redshifted to $z = 6.8$ and with the characteristic absorption trough imposed blueward of redshifted Ly- α (solid black curve). For comparison the spectra of cool M8- and T5-dwarfs are also plotted (dash-dot and dashed curves respectively).

to near-IR high- z quasar selection in visual form. In Figure 2 a Z, Y, J colour-colour diagram is presented with the derived synthetic photometry. The quasar tracks are colour coded according to their redshift, in steps of $\Delta z = 0.01$ and the average track is labelled at various redshifts for clarity. The box bounded by the dashed line illustrates the general principle; the box includes almost all $6.5 \leq z \leq 7.5$ quasars, rejecting galaxies as shown by the E1 locus (Rowan-Robinson et al. 2008) and almost all foreground stars.

The position of each quasar in Z – Y is a function of redshift, reflecting the movement of the Ly- α break through the Z-band. The Y – J colours have only minor dependence on redshift until $z = 6.9$ where the locus begins to turn over as Ly- α enters the observed Y band. Conversely, the distribution of stellar colours is driven largely by temperature, which acts to redden spectral types approaching early-L. In later types, behaviour is more complicated as clouds act to mask spectral features and redden near-IR colours (see Kirkpatrick 2005). With the appearance of pressure broadened NaI and KI doublets in the reddest optical bands at mid to late L, the sequence is forced redward in Z – Y into the T sequence.

The simple cuts outlined above will need to be modified for a real survey, since random photometric errors will broaden the measured locus, and thus can scatter stars and galaxies into the quasar selection region. Since all stars and galaxies outnumber genuine high- z quasars by a factor $> 10^6$ ($J \lesssim 21$), a realistic survey will need to ensure that the cuts are sufficiently far from the stellar locus to reject almost all stars and galaxies. In the remainder of this article we examine how best to place these cuts such that they isolate the vast majority of high- z quasars without selecting unacceptable numbers of contaminants.

3 Z, Y OFFSETS FROM THE VEGA SYSTEM

VISTA photometry is calibrated with reference to a set of 2MASS (the Two Micron All-Sky Survey; Skrutskie et al. 2006) standards, which have been measured with reference to the spectrophotometric standard star Vega (α -Lyrae). This implies that Vega is a zeroth magnitude star in all VISTA bandpasses. The calibration involves measuring the

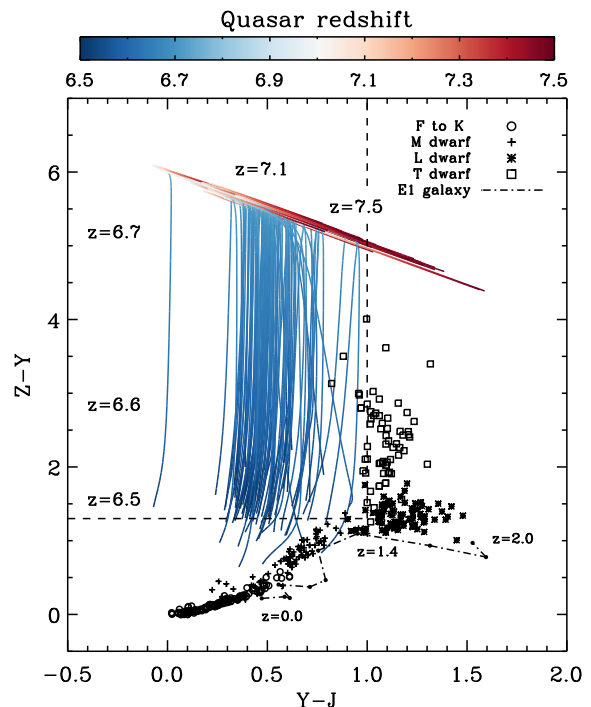


Figure 2. The Z, Y, J colour plane; high- z quasar redshift evolution tracks are colour coded as indicated by the colour bar. Star and galaxy colours are indicated by the legend. The dashed line describes the general principles of quasar colour selection in the Z, Y, J passbands, enclosing the vast majority of high- z quasars while rejecting the vast majority of galaxies and foreground stars.

offsets between the 2MASS standards and VISTA observed stars via a set of colour equations. Since 2MASS photometry was measured in the J, H, Ks bands alone the basic assumption is that the 2MASS colour equations can be linearly extrapolated to cover the VISTA Z and Y bandpasses. Any divergence from linearity will result in an offset from the Vega system in the extrapolated wavelength region.

A similar occurrence was noted by Hodgkin et al. (2009) in UKIDSS data release 2, where a rigorous analysis

of the Z, Y, J, H and K photometry against the overlapping SDSS footprint found a significant offset in the Y-band. A similar analysis for VISTA will no doubt be attempted when the catalogues are diverse enough to make precise measurements. However, since our quasar selection criterion is to be partly based on Vega zeroed synthetic photometry, it is important to at least tentatively determine any offsets present before we begin.

VIKING data is processed by the VISTA Data Flow System (Emerson et al. 2004) in its pipeline (Irwin et al. 2004) and retrieved from the VISTA Science Archive⁸ (VSA; Hambly et al. 2004). At the time of this analysis the VSA contains the latest v1.0 VIKING release which comprises of some 200 deg² of imaging in Z, Y, J and 120 deg² of imaging in all five bands; 90 deg² of this has complementary SDSS overlap. Offsets in this data set are measured following the approach of Hodgkin et al. (2009), the main points of which are summarised here. The reader should refer to the original paper for a full description including the maximum likelihood fitting procedures referred to below.

A sub-sample of high signal-to-noise ($S/N \geq 10.0$) point-like sources detected in both VIKING and the SDSS was defined and those sources with Vega like SDSS colours i.e. A0 stars with $u - g$, $g - r$, $r - i$ and $i - z$ in the range -0.1 to 0.1 , were flagged. Figure 3 plots the J, H and Ks colour-colour diagram for this set of sources. Blue points show the photometrically selected sample of A0 stars. The small number of these objects highlights the difficulty of investigating the VIKING colours at this early stage. The median colours of this sample are $J - H = 0.005 \pm 0.038$ and $H - Ks = 0.033 \pm 0.023$ (where the median absolute deviation has been used to estimate the standard deviation), which perhaps hints at small offsets in one or both of H/Ks. Given that each of these colours has been directly calibrated from 2MASS standards, we continue our analysis assuming that any offset in these passbands is small. As we will show shortly, there is evidence that this assumption is a good one. Also plotted in Figure 3 are red crosses, which show the synthetic colours of the stellar sequence derived from the Bruzual-Persson-Gunn-Stryker (BPGS) spectroscopic atlas (Gunn & Stryker 1983) in Section 1. The synthetic locus is in overall good agreement with the locus of bright stars in this colour-colour space.

Following Hodgkin et al., we now extend the baselines on each Z, Y, J, H and Ks colour-colour combination in one direction by plotting all possibilities against $u - Ks$. Offsets from zero are then measured from straight line fits to the data. To clarify this procedure an example of the fitting in the Z, J, u and Ks colour plane is shown in Figure 4. Due to limited statistics our approach to the fitting differs slightly from Hodgkin et al. (2009) who bin their data and take measurement errors based on standard deviations on binned median values. Conversely our approach is to fit to the photometrically selected A0 stars and retrieve errors directly from the maximum likelihood fitting procedure.

⁸ The VSA holds the image and catalogue data products generated by the VISTA Infrared Camera (VIRCAM). The primary contents of the archive originates from the VISTA Public Surveys. The archive can be queried via the Structured Query Language (SQL) and several interactive web forms at <http://horus.roe.ac.uk/vsa/index.html>

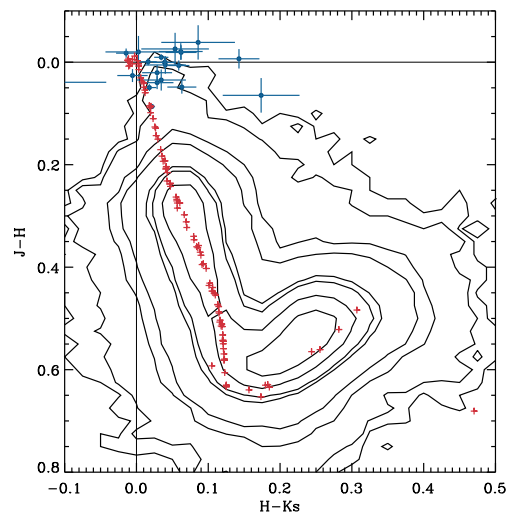


Figure 3. The VIKING J, H, Ks colour plane for high confidence stellar sources matched in VIKING and SDSS. Blue points are stars with Vega like colours in all SDSS passband combinations. Red crosses are synthetic photometry from BPGS spectroscopic atlas (Gunn & Stryker 1983).

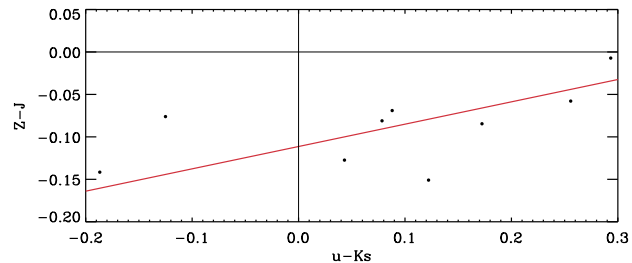


Figure 4. Maximum likelihood fit to stars with Vega like colours in SDSS with counterparts in VIKING. Similar fits were made in all other VIKING colour combinations vs. $u - Ks$, the results are summarised in Table 1 and in the main text.

The results show appreciable offsets in the Z and Y bands only. These are summarised in Table 1. The corresponding offsets found in the J, H and Ks bands are consistent with zero; $\Delta_{JH} = 0.006 \pm 0.004$, $\Delta_{JKs} = 0.008 \pm 0.005$, $\Delta_{HKs} = 0.013 \pm 0.006$.

A further two results are shown in Table 1, these were obtained by fitting to the blue end of the stellar locus from all the bright stars in the original selection. Again a straight line maximum likelihood fit is applied in the Z, J, Ks and Y, J, Ks colour-colour spaces and the offsets from the origins are measured. The best fitting line to the Z, J, Ks stellar locus is shown in Figure 5 and the measured offsets in both the Z, J, Ks and Y, J, Ks colour spaces are summarised in Table 1. In these cases the measured offsets are slightly larger than those measured in the VISTA-SDSS colour-colour spaces. These may well be attributed to small offsets in the J or Ks passbands as tentatively suggested by Figure 3. Individual offsets to the J, H and Ks passbands implied by these fits are clearly smaller than those attributed

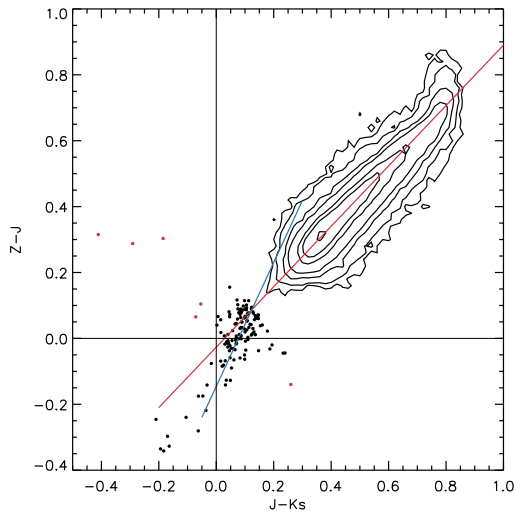


Figure 5. The VIKING Z, J, Ks colour plane for high confidence stellar sources matched in VIKING and SDSS. A sample of blue stars is plotted with filled circles, obvious outliers were clipped from the sample and are shown in red. The blue line shows the maximum likelihood straight line fit to this distribution, while the red line shows the fit to the main sample. The Z band offset is measured from the blue star intercept to the origin.

	Δ_Z	Δ_Y
Δ_{ZJ}, Δ_{YJ}	-0.111 ± 0.002	-0.082 ± 0.002
Δ_{ZH}, Δ_{YH}	-0.109 ± 0.004	-0.086 ± 0.004
$\Delta_{ZKs}, \Delta_{YKs}$	-0.096 ± 0.006	-0.073 ± 0.005
$\Delta_{ZJKs}, \Delta_{YJKs}$	-0.146 ± 0.003	-0.135 ± 0.003
Mean	-0.116 ± 0.008	-0.094 ± 0.007

Table 1. Summary of Z and Y offsets from the Vega system.

to Z and Y and will not present significant problems in the following sections.

4 MODELLING THE VIKING SURVEY

Having used synthetic photometry to predict the colours of cool stars and quasars in the VISTA Z, Y and J bandpasses, the next step is to combine this information with number count models of the cool-star and quasar populations to produce a simulation of the Z, Y and J band photometry expected from VIKING.

4.1 Quasar number counts

It is well established that the space density of quasars peaks at $z \simeq 2.5$ and declines rapidly thereafter (e.g. Richards et al. 2006). By $z \sim 6$ there are ~ 400 quasars brighter than $z = 21.0$ over the entire sky. Since the aim of this work is to limit our follow-up observations to a manageable number of objects, the specific number of quasars expected from VIKING is not directly relevant because the overwhelming majority of follow-up candidates

will not be quasars at all. Nevertheless, the calculation is important for two other reasons; firstly to demonstrate that follow-up at this stage presents a statistically viable prospect of discovering a quasar and secondly because doing so will allow qualitative constraints to be placed on the luminosity function when the VIKING quasar search begins to bear fruit.

The number of quasars brighter than an apparent magnitude m_p in some fixed observing passband p over a given redshift interval may be calculated via integration of the quasar luminosity function (QLF) over comoving volume to a depth given by the absolute magnitude limit of the survey. The latest determination of the QLF at $z \simeq 6$ was undertaken by Willott et al. (2010) and combines discoveries from the CFHQS with the more luminous SDSS main and deep samples. The input catalogue comprises of 40 quasars sampling the redshift range $5.74 < z < 6.42$. The bright end of the binned luminosity function is well constrained to a power law with some evidence for a flattening in the slope provided by a single quasar at lower luminosities. In keeping with work at lower redshifts, where the QLF is well constrained over a large magnitude interval (Boyle et al. 2000; Croom et al. 2009; Glikman et al. 2011), the Willott et al. parametric QLF has a double power law form.

At $z \simeq 6$, the space density of bright SDSS quasars ($M_{1450} \lesssim -27$) measured by Fan et al. (2001) is consistent with a single power law extrapolation of the QLF between $3 \leq z \leq 5$ (Schmidt et al. 1995). The rate of evolution implied by these luminosity functions corresponds to a value $k = -0.47$, where the space density declines exponentially as $10^{k(z-6)}$. Beyond $z \simeq 6$ the value of k is of course completely unknown and moreover one cannot rule out the possibility of a noticeable luminosity dependence, similar to those inherent in quasar, AGN and galaxy populations at lower redshifts (Cowie et al. 1996; Barger et al. 2005; Croom et al. 2009). Clearly then, by extrapolating much past $z \simeq 6$ one should only make baseline projections.

We compute a baseline number count model adopting the value $k = -0.47$; we also compute the extreme cases $k = 0$ (no evolution model) and $k = -0.94$, which corresponds to a factor 3 decline in density per 0.5 increase in redshift. Model number count curves are shown in Figure 6, which also includes open circles at the inverse area of VIKING, the UKIDSS-LAS and the VISTA Hemisphere Survey (VHS) at their respective 10σ sensitivity limits i.e. the surface density at which the given survey would contain a mean of one quasar. Shaded regions indicate the change in number counts when the faint end slope of the QLF ($\beta = -1.5$) is allowed to vary between $-2.0 \leq \beta \leq -1.0$. The small deviations from the initial models show that VIKING will probe the bright end of this specific QLF. The baseline model predicts ~ 8 $z \geq 6.5$ quasars brighter than the 10σ sensitivity limit over the entire VIKING field, which would correspond to a total of ~ 2 quasars in the first 350 deg^2 of imaging.

The UKIDSS eighth data release (DR8) contains some 2600 deg^2 of LAS imaging in at least the Y- and J-bands. The baseline number count model predicts that there should be a mean of two $z \geq 6.5$ quasars in this area, while the non-evolving model predicts ~ 3 . At present there is one reported discovery of a $z \geq 6.5$ quasar ($z \simeq 7$ to be a little

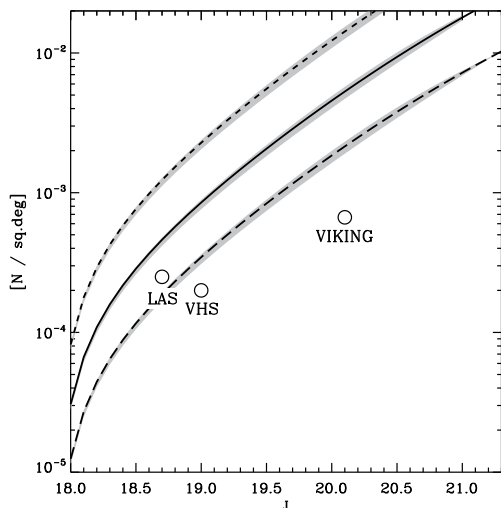


Figure 6. The number of $6.5 \leq z \leq 7.5$ quasars brighter than J , for three models based on the luminosity function of Willott et al. (2010). The parameter k determines the rate of density evolution beyond $z = 6$. The short-dashed, solid and long-dashed curves correspond to $k = (0.0, -0.47, -0.94)$ respectively (see text for details). Open circles have been placed at the inverse area of various surveys, showing the surface density at which the given survey would contain a mean of 1 quasar brighter than its 10σ detection limit. Shaded regions show the deviations in each curve when the faint end slope ($\beta = -1.5$) is allowed to vary between $-2.0 \leq \beta \leq -1.0$.

more precise) in UKIDSS DR8 (Mortlock et al. 2011), which marginally favours the evolving models.

4.2 Stellar number counts

The Besançon stellar population synthesis model of the Galaxy (BGM; Robin et al. 2003; Robin & Reylé 2003) allows stellar number counts up to spectral type M to be computed as function of J-band magnitude and direction on the sky via an interactive web form⁹. The model is currently undergoing an update to the set of M-dwarf atmospheres it uses. The current study therefore provides an ideal testbed in which to compare their performance. Here we briefly review the model inputs and the changes to the M-dwarf atmospheres.

The atmospheres of cooler L- and T-dwarfs are much less well constrained and so we take a more empirical approach to calculate their number counts.

4.2.1 The Besançon Stellar Population Synthesis Model of the Galaxy: M-dwarf number counts

The Besançon Galaxy Model has been designed to produce simulations of the stellar content in the Galaxy as seen towards different lines of sight and photometric bands. It is based on assumptions about stellar evolution, Galactic evolution and Galactic dynamics. The model includes 4 populations (thin disc, thick disc, halo and bulge) each one deserving

⁹ <http://model.obs-besancon.fr/>

ing a specific treatment. The main ingredients to simulate those populations are the density laws, the initial mass function (IMF) and the star formation rate.

At the magnitudes considered here, the more relevant parameters to estimate counts of M-dwarf stars are the slope of the IMF at low masses and the scale height. Thin disc scale height has been obtained from a dynamical argument; the scale height depends on the local density, the age-velocity dispersion relation and the potential through the Boltzmann equation. Hence the thin disc scale height is fixed for an isothermal population of a given age and a given vertical velocity dispersion. The different scale heights or ellipticities as a function of age are given in Robin et al. (2003).

The IMF used in the simulations is different from the BGM on line, which was obtained in an analysis in Schultheis et al. (2006) where the slope of the IMF in the thick disc has been found to be very steep. Later on this IMF was discarded when compared with deep data because it overestimated numbers of M-dwarfs in the simulations. This mistake was probably due to a default of the calibration of the model in the Canada France Hawaii Legacy Survey (CFHTLS) bands. The IMF slope has now been revised and we use here a slope of $\alpha = 0.7$ down to very low masses, as in Haywood et al. (1997) where the IMF is parametrised as $dN/dM \propto M^{-(1+\alpha)}$.

The computations of the magnitudes and colours of the stars rely on the stellar atmosphere models. Despite of the fact that the Basel library was used for most of the HR (Hertzsprung-Russell) diagram (Lejeune et al. 1997), for low mass stars those models significantly deviate from observations (Schultheis et al. 2006). Instead we use NextGen model atmospheres (Allard et al. 1997) at effective temperatures smaller than about 4000 K. At the present time, the BGM does not include brown dwarfs of masses smaller than the hydrogen burning limit.

Stellar number counts were calculated on a 2D grid of spectral-type and J-mag bins for 30 representative fields of 10 deg^2 for each of the thin-disc, thick-disc and halo components. The results were scaled up accordingly. In order to make certain that density gradients were well sampled, effort was made to ensure that each field was offset from adjacent fields by no more than 5 deg of Galactic latitude. J-band number counts were then calculated in the range $16.0 \leq J \leq 24.0$ in bin widths of $\Delta J = 0.5$. According to the quasar number count model this is ~ 2 mag brighter than we can realistically expect to recover quasars in VIKING and ~ 3 mag fainter than the 5σ limiting magnitude of the survey. The extra range is included to allow sources to scatter in and out of the survey as the result of photometric error.

4.2.2 L- and T-dwarf number counts

For number counts of L- and T-dwarfs one can consider the standard empirical Galactic density model, whereby the total contribution from the thin and thick discs is given by the sum of two double exponential profiles (e.g. Chen et al. 2001). A full description of the number count calculation is provided by Caballero et al. (2008) so here only the main points are reviewed.

The space density of either disc component at Galactic

Table 2. Parameters of the Galactic thin and thick disc system (Chen et al. 2001; Jurić et al. 2008)

R_{\odot} (pc)	Z_{\odot} (pc)		L (pc)	H (pc)
8600 ± 200	$+27 \pm 4$	Thin:	2250 ± 1000	330 ± 3
		Thick:	3600 ± 720	$580 - 750$
		Thick disc normalisation: 13 - 6.5 %		

coordinates (l, b) and heliocentric distance d assumes the following form

$$n(d, l, b) \propto \exp\left(-\frac{R(d, l, b) - R_{\odot}}{L}\right) \exp\left(-\frac{|Z_{\odot} + d \sin b|}{H}\right), \quad (1)$$

where Z_{\odot} is the position of the sun relative to the Galactic plane and H and L represent the scale height and length of the particular disc component. Since VIKING observes extra-galactic fields i.e. out of the Galactic plane, the assumption $R_{\odot} \gg d$ is valid and the galactocentric distance at the point of interest $R(d, l, b)$, is given by the approximation

$$R(d, l, b) \approx R_{\odot} - d \cos b \cos l. \quad (2)$$

The proportionality constant is the spatial density of the relevant object class or classes at $Z = 0$ i.e. at the Galactic plane.

We adopt the local space density and absolute J-band magnitude per spectral type estimates of Caballero et al. (2008) and calculate stellar number counts per spectral type in J-magnitude bins of width 0.5 over the range $16 \leq J \leq 24$. The parameters for the thin and thick discs are taken from Chen et al. (2001) and Jurić et al. (2008) as given in Table 2.

We assume an identical luminosity function in both the thin and thick discs. This probably overestimates the count of thick-disk brown dwarfs, since old population sub-stellar objects are predicted to have very faint magnitudes by theoretical cooling sequences (Kirkpatrick 2005). This would place most of the thick-disk population with $M < 0.06 M_{\odot}$ below VIKING detection limits. This assumption is therefore conservative since it will overestimate the brown-dwarf contamination of the quasar sample.

A similar argument can be made for the halo, which represents an even older population. In this case we assume that all halo L- and T-dwarfs will be below VIKING detection limits. BGM number counts of halo M-dwarfs fall off rapidly towards cooler spectral types. The BGM surface density of halo M9-dwarfs with $J < 23.0$ is $< 1 \text{ deg}^{-2}$, suggesting that this is a reasonable approach.

4.3 Generating Synthetic Observations

With stellar number counts binned by apparent J-band magnitude and spectral type, the next step is to pair each count with a set of synthetic photometry to mimic an observation of each source.

For N sources distributed over $J_1 \dots J_p \dots J_P$ magnitude and $T_1 \dots T_q \dots T_Q$ spectral type intervals, the procedure is to step over all $P \times Q$ bins iteratively. Each object receives a set of synthetic fluxes given by $\mathbf{F} = (f_Z, f_Y, f_J)$. $\tilde{\mathbf{F}}$ is then generated via interpolation of our synthetic photometry (Section 2) between a source of the relevant spectral type T_q and that of the later adjacent spectral type, T_{q+1} . If the r th occupant of bin p, q has a magnitude J in the range $J_p \leq J < J_{p+1}$ and a spectral type T_q , then $\tilde{\mathbf{F}}$ is defined by the following weighted sum:

$$\tilde{\mathbf{F}} = \alpha \mathbf{F}_{p, q, r} + (1 - \alpha) \mathbf{F}_{p, q+1, r}, \quad (3)$$

where α is a uniform random deviate in the range $0 < \alpha \leq 1$. Each of the components of $\tilde{\mathbf{F}}$ (i.e. $\mathbf{F}_{p, q, r}$ and $\mathbf{F}_{q, q+1, r}$), comprise of Z-, Y- and J-band fluxes generated by drawing Z- and Y-band fluxes from our library of synthetic photometry for the relevant spectral type. These are then scaled to a reference flux f_J , which is derived from a magnitude J drawn randomly from the interval $J_p \leq J < J_{p+1}$. This process is repeated over all $P \times Q$ bins until all number counts are coupled to a set of unique synthetic photometry.

The VSA VIKING release v1.0 currently contains 173 image tiles. During the image reduction and pipeline processing the average sky noise in each image tile is measured by placing a number of circular apertures in sparsely populated regions. These measurements are then placed in the header units of each image before being uploaded to the VSA. In a real survey of faint sources the distribution of measured flux errors is sky dominated and usually well approximated as being Gaussian. The intrinsic distribution of synthetic fluxes can therefore be perturbed by drawing from a set of Gaussian distributions, with standard deviations equal to the sky noise level in the VIKING image tiles and scaled to the theoretical flux of the object in the corresponding passband. Adding this distribution of errors to the set of simulated intrinsic fluxes gives a set of simulated ‘observations’.

4.4 Generating a Synthetic Catalogue

The catalogue extraction process for the VIKING survey, is handled by the VISTA Data Flow System (VDFS) at the Cambridge Astronomical Survey Unit (CASU). The CASU source extraction algorithm does not implement a rigid detection threshold. Thus to determine whether our synthetic sources would be detected by the CASU source extractor it is necessary to model the S/N distribution of detected sources from the data. Here we follow a novel method used by Patel (2010), which is described in brief below.

Since we are modelling a population of point sources it is necessary to limit the data analysis to stars only, which requires a highly reliable method of star-galaxy separation. In contrast to Patel (2010), who used morphological classifiers to define a reliable and complete sample of point-like objects, here we use colour separation by matching sources in VIKING, the VISTA Deep Extra-galactic Observations survey (VIDEO) and the CFHTLS. These surveys share an overlap region of $\sim 1 \text{ deg}^2$ in the VIDEO tile centred on $\text{Ra} = 02^{\text{h}} 26^{\text{m}} 00^{\text{s}}$ and $\text{dec} = -04^{\circ} 30' 00''$ (the VIDEO-XMM3 field). VIDEO observes in the same passbands as

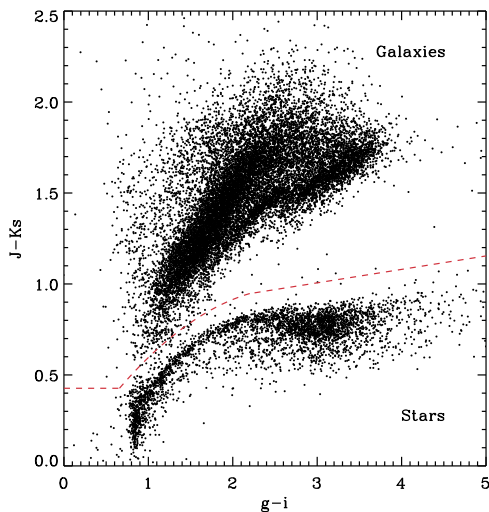


Figure 7. The CFHTLS-VIDEO g , i , J , K_s colour plane for matched VIKING-VIDEO-CFHTLS sources in the $\sim 1 \text{ deg}^2$ region of overlap shared by each survey. The deep CFHTLS-VIDEO observations allow robust star galaxy separation. The red dashed line shows the regions in which the star and galaxy populations are defined.

VIKING but is ~ 2.5 mags deeper (5σ limiting depths of $Z = 25.2$, $Y = 24.0$, $J = 23.6$, $H = 22.6$ and $K_s = 21.7$). At the time of writing only the Y , J , H and K_s observations are available, but this is not important since most high- z quasars will be too faint to be detected in VIKING Z -band observations given the CASU $\sim 5\sigma$ extraction criterion.

The CFHTLS Deep survey observes in the Sloan passbands to limiting depths of $u = 26.6$, $g = 28.0$, $r = 27.6$, $i = 27.0$ and $z = 25.7$. Sources matched between all three surveys are plotted in the CFHTLS-VIDEO $g - i$ vs. $J - K_s$ plane in Figure 7. The extra depth in the matched catalogue minimises photometric scatter and, with the combination of colours, gives remarkably good star galaxy separation. The red dashed line in Figure 7 separates two regions from which we draw a sample of stars and galaxies. Where possible i or g dropouts have been classified by virtue of either their $z - J$ vs $J - K_s$ colours or their $J - K_s$ colours alone. In this section we concentrate on the stellar sample.

Histograms of the J -band magnitude distributions of matched stars are shown in Figure 8 for VIKING (red) and VIDEO (blue) photometry. For comparison, the full distribution of VIDEO-CFHTLS matched point sources is also plotted (black histogram). Synthetic sources are drawn randomly from this distribution and each source is perturbed by a Gaussian error with a standard deviation equal to the sky-noise level drawn from VIKING image tiles. Each perturbed source is then given a detection significance (S/N) threshold drawn from a Gaussian distribution with mean μ_p and standard deviation σ_p . If a given source possesses a S/N greater than its simulated detection threshold then it is kept otherwise it is discarded. The resulting distribution is then compared by eye to the VIKING-VIDEO-CFHTLS matched distribution and the process is repeated with various values of μ_p and σ_p until a good match is found. The continuous black curve in Figure 8 shows the accepted matched J -band

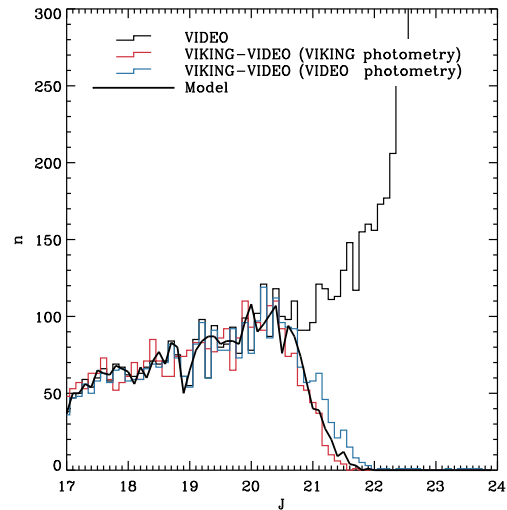


Figure 8. The J band magnitude distributions of sources matched between VIDEO-CFHTLS (black histogram) and VIKING-VIDEO-CFHTLS with VIKING photometry (red histogram) and with VIDEO photometry (blue histogram). The black continuous curve shows the distribution of simulated sources with intrinsic magnitudes drawn from the VIDEO-CFHTLS matched catalogue and perturbed with realistic VIKING-like Gaussian errors. A Gaussian distributed signal to noise cut has been applied to mimic the source extraction process used to produce the VIKING catalogue (see text for details).

distribution with the parameters $(\mu_J, \sigma_J) = (0.22, 0.04)$. The same procedure was undertaken in the Y -band yielding a Gaussian with parameters $(\mu_Y, \sigma_Y) = (0.15, 0.06)$. The findings were applied to the set of simulated observations described above resulting in a realisation of the cool star component of the VIKING catalogue over the entire 1500 deg^2 of the VIKING field.

5 THE Z , Y , J SELECTION CRITERIA

The magnitude and colour distribution of the simulated stellar population has been compared with data from the VIKING-VIDEO-CFHTLS catalogue. The results are shown in Figure 9, where we plot the real data in histogram format and the simulated catalogue as smooth curves. An excess of blue stars can be seen in the colour distributions in the left hand panels. Closer inspection of the magnitude distribution of these stars shows that they are reasonably faint with number counts peaking at $Z \sim 19.5$, $Y \sim 19.5$ and $J \sim 19.0$. Given their blue colours, they are likely intrinsically bright main sequence halo stars. To promote a fair comparison between the true and modelled magnitude distributions an effort has been made to remove the majority of the blue stars from the data by retaining only those having $Z - Y \geq 0.0$, $Y - J \geq 0.0$, $Z - J \geq 0.3$.

The overall agreement between colour and magnitude distributions in the model and the data is good, but the model over predicts the number counts in some bins by up to a factor of 1.3. The number count predictions are therefore conservative. In the modelled population almost all objects

are M-dwarfs whose number counts and J-band magnitudes are predicted by the BGM. Given the rarity of cooler type objects, the 1 deg^2 patch of deep VIKING-VIDEO-CFHTLS matched imaging is not sufficient to constrain the L- and T-dwarf number count model well. The overall good agreement with the data suggests that for the latest type dwarfs, the modelled objects are distributed accurately over colour and magnitude space and that the predicted number counts are within an order of magnitude of their true values. It is also encouraging that our results broadly conform with data from recent near-IR searches (Burningham et al. 2010; Lodieu et al. 2009). With a set of well placed colour cuts, L- and T-dwarfs are known to make only modest contributions to high-z quasar candidate lists in comparison to M-dwarfs, so the propagation of these uncertainties will not have a large impact on estimates of quasar colour space contamination.

In the following section the modelled stellar and quasar photometry are employed along with data from the VIKING-VIDEO-CFHTLS overlap region to investigate contamination to quasar colour space and to lay down some benchmark selection criteria relevant to the first candidate follow-up run. We emphasise the use of the word ‘benchmark’ here to mean that we will be working conservatively, placing tighter constraints than will perhaps be necessary. In a real survey it is often useful to relax constraints e.g. so that one can consider the errors on candidates around the selection cutoff boundaries.

5.1 Contamination of quasar colour space

Take as an illustrative example the first follow-up of VIKING quasar candidates, which was scheduled over three nights in June 2011. As a rough estimate one might expect this to be sufficient to make ~ 100 observations. Prior to this, there was expected to be $\sim 300 \text{ deg}^2$ of data available from which to choose candidates. This allowed us to set a first broad-brush selection constraint e.g. that we must limit our follow-up catalogue to ~ 1 candidate per 3 deg^2 . To place further, similar benchmark constraints it is necessary to look in more detail at contamination of quasar colour space.

5.1.1 Extra-galactic Contamination

Up to now, the focus of this work has been on contamination from foreground Galactic M-, L- and T-dwarfs. Referring back to Figure 2 it is clear that contamination from Galaxies could also pose a problem. Fortunately most galaxies can be rejected on the basis of their extended disc-bulge morphologies. At faint magnitudes, it is possible for the galactic disc component to fall below the detection limit of the survey, while the bulge component remains bright. Galaxies detected in this way can be morphologically indistinguishable from stars and usually the best way to avoid this type of contamination is to apply a detection significance constraint to ensure that candidates are sufficiently well detected in at least one band.

The star galaxy separation techniques discussed in the previous section present the opportunity to study the statistical properties of VIKING galaxies in detail and place further selection constraints on both the morphology and

detection significance of quasar colour space contaminants. The resulting galaxy sample is on the whole slightly less reliable than the stellar sample, since it shares a similar region of colour space with low-z ($0.1 \leq z \leq 2.5$) quasars. The lack of any SDSS spectroscopic overlap prevents any attempts to remove these interlopers with any confidence, but work on optical and near-IR number counts (e.g. Richards et al. 2006; Maddox et al. 2008) suggests that low-z quasars will be outnumbered by galaxies in this sample by at least two orders of magnitude and they can be reasonably neglected.

The VSA provides a number of morphological classifiers based on the curve of growth of the individual detections of each source in a set of progressively inclusive apertures. The finer details of this approach are discussed extensively by Irwin et al. (In preparation), the main points are summarised as follows; measurements are made on ellipticity and curve-of-growth statistics. The results are then compared at the detector level to the average stellar locus as a function of magnitude. In this way each detection is given a morphological classification statistic known in the VSA as the merged-ClassStat (MCS). For stars, this statistic is well approximated by an $N(0, 1)$ Gaussian distribution. Each individual classification is combined to give the overall classification for each source.

At bright magnitudes stars and galaxies populate two separate and well defined MCS loci. At faint magnitudes the galactic locus becomes indistinguishable from the stellar locus. We add to the sample of stars and galaxies, a sample of objects which are unmatched between VIKING and VIDEO and label these sources as ‘noise’. Figure 10 shows the completeness and contamination of the stellar sample by galaxies and noise within the following constraints; $-10 \leq \text{MCS} \leq 10$ (solid curve), $-7 \leq \text{MCS} \leq 7$ (dotted curve), $-5 \leq \text{MCS} \leq 5$ (dashed curve) and $-3.5 \leq \text{MCS} \leq 3.5$ (dash-dotted curve). It is clear that losses in completeness are small compared to gains in minimising contamination. However even with the tightest constraints contamination contributes to ~ 60 per cent of the sample at the faintest magnitudes.

The VSA supplies a second useful morphological classification statistic called the pClass. pClass is derived from a discrete statistic which allocates a classification based on the passband level MCS and several catches to make classification more reliable (e.g. for saturated sources). Each discrete classification corresponds to a reasonably accurate, self-consistent probability for each of the allowed cases; star, galaxy, noise and saturated. For each source the pClass statistics for each separately available detection are then combined using Bayesian classification rules assuming independence. This defines the probability that a given source is either a star, galaxy, noise or saturated, the relevant attributes in the VSA being pStar, pGalaxy, pNoise and pSaturated.

The sources in our matched VIKING-VIDEO-CFHTLS catalogue are all fainter than $J = 17.0$ and so in all cases $\text{pSaturated} = 0.0$ and $\text{pStar} + \text{pGalaxy} + \text{pNoise} = 1.0$.

We place the following cuts on each of the morphological classifiers,

$$\begin{aligned} \text{pNoise} &\leq 0.6 \\ \text{pGalaxy} &\leq \text{pStar} + 0.9 \end{aligned}$$

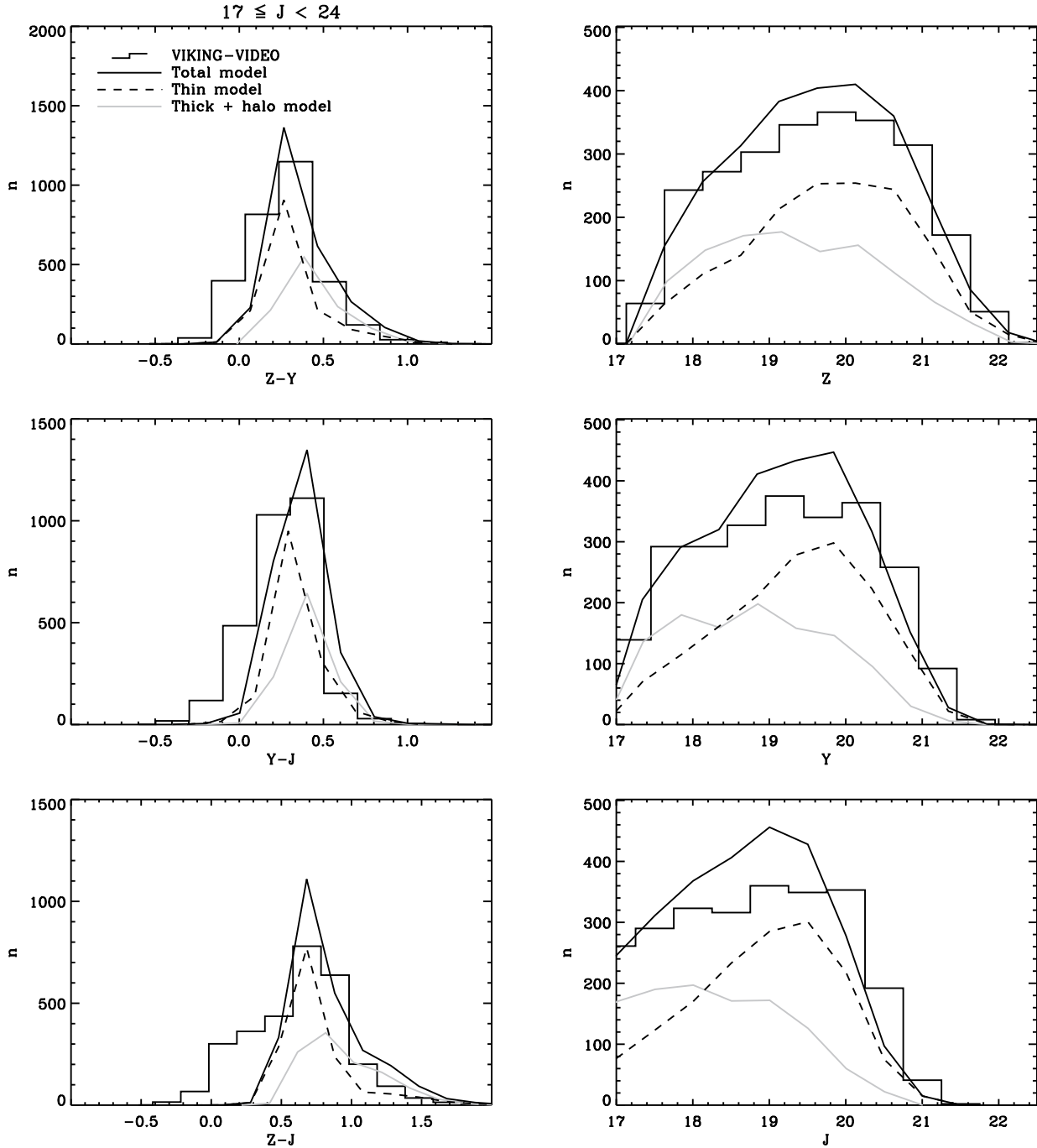


Figure 9. Left: VIKING Z, Y, J colour distributions of the simulated thin disc, combined thick disc and halo and total cool star contributions in $\sim 1 \text{ deg}^2$ of the VIKING-VIDEO-CFHTLS overlap region. Each distribution is compared to the real distribution of VIKING stellar photometry as shown by the histogram style plots. The excess of blue objects in each plot is attributed to main-sequence halo stars with bright absolute magnitudes, an effort has been made to remove these objects in order to compare modelled and true magnitude distributions. Right: As in the left hand panel but for the simulated and real Z, Y, J magnitude distributions. In both cases the overall agreement with the data is good. There is a slight overshoot in predicted number counts making these models conservative.

and in Figure 10 the contamination and completeness of the stellar sample is plotted in grey for $-3.5 \leq \text{MCS} \leq 3.5$. With the new constraints the contamination from galaxies is significantly reduced with only a small reduction in completeness as the penalty.

Figure 11 (a) plots all galaxies in the Z, Y, J plane and galaxies passing the morphological constraints are plotted in panel (b). Given the morphological constraints the remaining galaxies in (b) are all indistinguishable from stars. We naturally want to select quasars as faint as possible, but

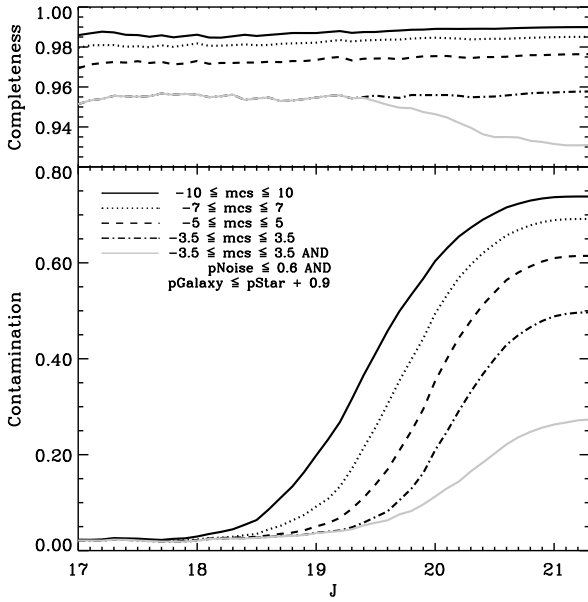


Figure 10. Upper: The completeness of VIKING-VIDEO-CFHTLS stellar sample with various morphological selection constraints imposed (see legend). Lower: The contamination of the VIKING-VIDEO-CFHTLS stellar sample by galaxies and noise with various morphological selection constraints imposed. All morphological statistics are derived from VIKING imaging.

experience from other surveys has shown that an 8σ to 10σ detection in at least one band is necessary to avoid the selection of large numbers of false positives (e.g. Fan et al. 2001). Therefore at the faint end we adopt a nominal photometric cut at $S/N \geq 8$ in both Y and J. Galaxies in Figure 11 passing this constraint are plotted in panel (c). Only a small fraction of the original galaxies remain and most are concentrated within the main galaxy locus. There are perhaps half a dozen sources lying sufficiently far from the galaxy locus to be mistaken for potential candidates. Since this is now the realm of small number statistics it is impossible to draw strong conclusions on the frequency of these or similar objects. Assuming that this distribution is typical for all VIKING galaxies, then in the worst case scenario all outliers from the locus would be considered for followup. This suggests, perhaps ~ 10 extra-galactic contaminants per deg^2 , although this is clearly a weak constraint. Better constraints can be placed on the extent of extra-galactic contamination when we begin to identify our candidates spectroscopically. For now, it is safer to work conservatively by placing a set of benchmark colour cuts such that all galaxies are rejected. These cuts are shown by the red dashed line in Figure 11.

5.1.2 Stellar Contamination

Figure 12 plots the simulated cool-star catalogue in Z, Y, J colour-colour space. Stars are represented as black points and contours. Plotted in blue as open circles is a catalogue of ~ 200 simulated $6.5 \leq z \leq 7.5$ quasars. Each source has been ‘detected’ at the 8σ level in Y and J and was drawn from larger catalogue of ~ 1000 quasars with a uniform dis-

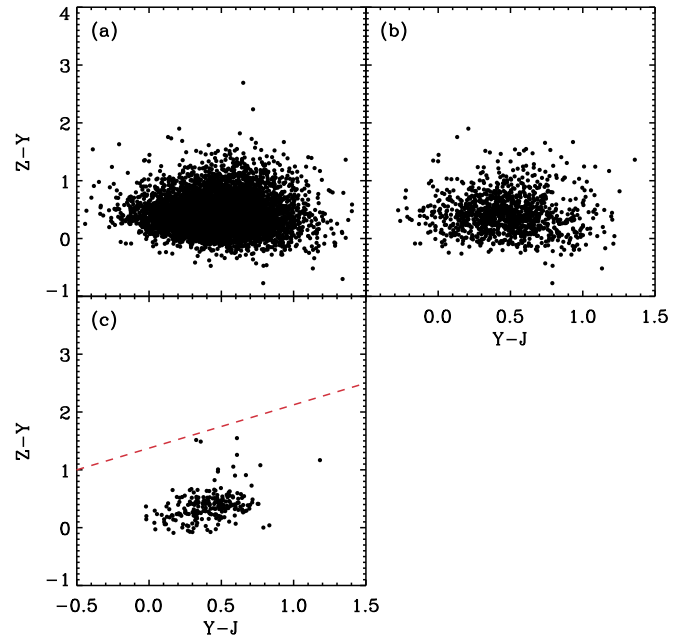


Figure 11. The VIKING Z, Y, J colour plane for a highly complete sample of galaxies selected from the VIKING-VIDEO-CFHTLS overlap region. Panel (a) shows all galaxies, Panel (b) shows remaining galaxies after morphological cuts have been imposed and Panel (c) shows the sample after both morphological cuts and an 8σ detection significance threshold in Y and J is applied. The red dashed line shows a conservative colour selection constraint, which rejects all remaining galaxies.

tribution in redshift. Given the selection space constraints derived in the previous section, the task here is simple; to refine these criteria to allow ~ 1 interloper per 3 deg^2 while simultaneously ensuring that the vast majority of quasars lie within these constraints. One also must ensure that the revised constraints do not constitute a relaxation of the above constraints.

The revised selection region is described by Equation 4 and shown in Figure 12 by the dashed line, which encloses ~ 500 interloping stars. As required, this corresponds to ~ 1 interloper per 3 deg^2 over the entire 1500 deg^2 of the VIKING field.

$$\begin{aligned} Z - Y &\geq 1.375 \\ Y - J &\leq 0.900 \\ Z - Y &\geq 0.750 (Y - J) + 1.375 \end{aligned} \quad (4)$$

Finally it is extremely important to verify whether these cuts maintain high completeness.

5.2 Selection Completeness

The estimated completeness contours of the selection strategy are shown as a function of J and redshift in Figure 13. Completeness is defined here as the fraction of catalogued quasars of intrinsic J-band magnitude J and redshift z, with observables that pass the morphological, significance and colour constraints outlined above. The total mean complete-

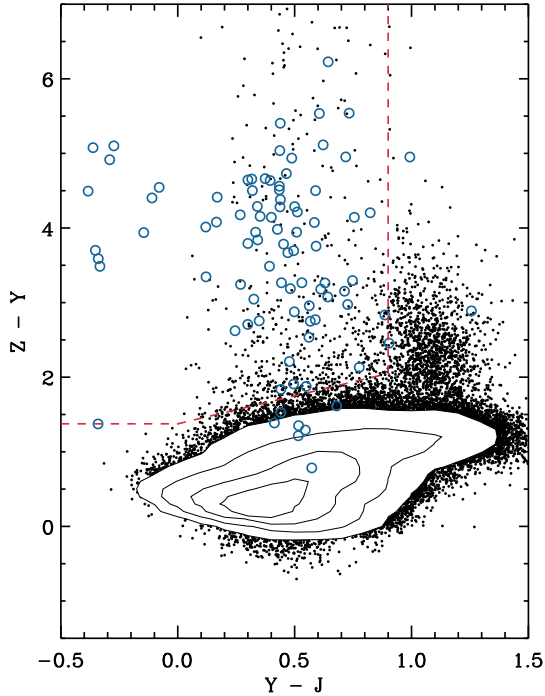


Figure 12. The VIKING Z , Y , J colour plane for simulated cool stars (contours and points) in the VIKING catalogue. Also shown are ~ 200 simulated $6.5 \leq z \leq 7.5$ quasars (open circles) drawn from a uniform distribution in redshift and ‘detected’ at the 8σ level in Y and J . The red dashed line defines a benchmark colour selection region that encloses ~ 1 object per 3 deg^2 as was required by the conditions of our follow-up campaign.

ness of the survey is ~ 60 per cent and is robust against moderate changes in the selection criteria that maintain the ~ 1 interloper per 3 deg^2 requirement.

The conservative selection constraints imposed on the simulated catalogue maintain a completeness that is comparable to but slightly lower than the highly successful SDSS and CFHTLS quasar searches in the optical and the UKIDSS search in the near-IR (Fan et al. 2003; Jiang et al. 2008; Willott et al. 2010; Patel 2010). The difference can be accounted for firstly by our conservative selection constraints and secondly because completeness estimations in these searches do not consider the losses due to morphological rejection. That said, it is important to mention that the completeness will be further affected by a few additional factors not modelled here. Firstly, loss of completeness due to survey ‘holes’ caused by ghosts around bright stars; secondly, blending with foreground objects causing genuine quasars to move bluewards in $Z - Y$ and be rejected and finally, non-Gaussian errors and spurious detections causing increased contamination compared to our models.

The bright-star losses are expected to be relatively small, rejecting typically a few percent of the sky. Secondly, the losses from chance projection of foreground objects are also modest; at $Z \sim 23$ the surface density of objects is ~ 10 per arcmin^2 , so if we assume (conservatively) real quasars will be rejected if closer than 2 arcsec to such an object, this will cause an inefficiency of 3.5 per cent.

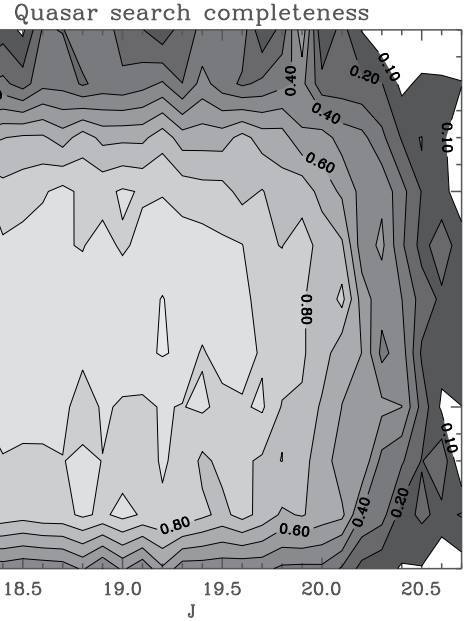


Figure 13. Estimated VIKING survey completeness for the benchmark selection constraints. Contours are plotted in J vs. z and increase in intervals on 0.1. The selection function accounts for loss of completeness from all significance, colour and morphological constraints described in the text.

Finally, there are many sources of non-Gaussian errors which may create spurious Z -dropouts, including moving objects such as asteroids, image persistence, hot pixels, etc. The VIKING observing strategy ensures that each object is observed at approximately 8 jitter positions on different pixels, and also that the J -band imaging is split into two epochs separated by weeks or months. Using this, we expect that almost all spurious, time-variable and moving objects can be rejected by checking of individual data frames, though the precise number remains to be quantified in detail.

With a mean completeness of ~ 60 per cent, the quasar number count models derived in Section 4, suggest that ~ 2 $6.5 \leq z \leq 7.5$ quasars brighter than the VIKING 8σ point-source sensitivity limit will be selected from the first $\sim 350 \text{ deg}^2$ of VIKING imaging, by the benchmark selection constraints.

6 NTT IMAGING OBSERVATIONS

The first VIKING quasar candidates were observed in I_{NTT} and Z_{NTT} imaging by the ESO Faint Object Spectrograph and Camera II (EFOSC2) on ESO’s New Technology Telescope¹⁰ (NTT) over a three night period between 26th - 29th June 2011. In practise both traditional colour selection and probabilistic candidate ranking (Mortlock et al. 2011) were employed independently to converge on the final candidate list and as recommended in Section 5 the benchmark colour and significance constraints were relaxed considerably in order to remain inclusive. Here we examine the VIKING Z , Y ,

¹⁰ Based on observations made with ESO Telescopes at the La Silla Paranal Observatory under programme ID 087.A-0655(A)

J photometry of these candidates and discuss implications for the benchmark selection constraints in light of the NTT observations.

In total 129 science exposures were taken of 44 candidates¹¹. All candidates were observed in I_{NTT} to depths of $\gtrsim 22.8$ mag at the 3σ noise level. At these depths $z \geq 6.5$ quasars are dark in optical passbands so candidates showing a visible flux peak in these images were discarded. In total just 6 candidates appeared undetected in I_{NTT} images that reached 3σ magnitude limits of $I_{NTT} > 23.7$ (this has since been confirmed with aperture photometry).

In Figure 14 the dashed line shows the benchmark selection region in the VIKING Z, Y, J colour-colour plane. The filled grey region shows the set of relaxed constraints used in the search. Dark grey points represent objects which pass the benchmark constraints but have not undergone follow-up. A small fraction remain strong candidates and are awaiting observation, but most were rejected after probabilistic ranking or because they are associated with an optical source in the SDSS overlap region. Crosses and open circles show I_{NTT} visible and I_{NTT} drop-out candidates respectively. As is clear from the scatter of these points outside of the grey region, even the relaxed constraints were not strictly adhered to.

The I_{NTT} drop-out lying at $Z - Y \simeq 1.25$, $Y - J \simeq 0.7$ is a faint ($S/N \simeq 6$ in Y) low-priority candidate and would not normally have been observed but for a nightly period in which most high priority candidates were not visible. Given its low priority it was not observed in Z_{NTT} . Excluding this object there remain five strong I_{NTT} drop-out candidates which were subsequently followed up in Z_{NTT} in order to confirm a break shortward of the VISTA Y-band. All were found to have a combination of colours in I_{NTT} , Z_{NTT} , Y and J consistent with $6.5 \leq z \leq 7.0$ quasars. Four of these candidates lie firmly within the benchmark colour selection constraints and a fifth lies on the boundary, three candidates lie just outside the significance constraints ($S/N > 7.3$; which serves as a reminder of the importance of widening the search space in order to consider the colour uncertainties on objects lying around the selection boundaries). The clustering of these candidates in and around the selection region provides considerable support for the choice of selection constraints. A detailed discussion and analysis of the NTT photometry, as well as the spectroscopy of these candidates is given by Venemans et al. (2011).

7 SUMMARY AND FUTURE WORK

The first public data release of the VIKING survey will be delivered to ESO in mid- to late-2011. Approximately 75 deg^2 is expected to be made public. VIKING is expected to contain a significant sample of $6.5 \leq z \leq 7.5$ quasars, the precise number depending sensitively on the unknown evolution of the quasar luminosity function beyond $z \sim 6$.

Follow-up of the first VIKING quasar candidates was conducted in June 2011. Candidates were chosen from \sim

¹¹ Given the modest area covered by VIKING at this stage ($\sim 350 \text{ deg}^2$), it should be noted that the observation run was heavily dictated by the visibility of the patchy VIKING footprint throughout the night. Thus the observations presented here do not represent an exhaustive list of our highest priority candidates.

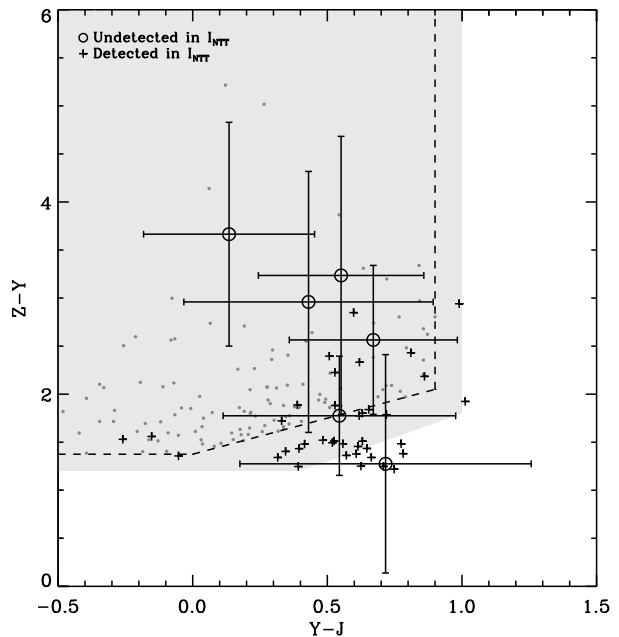


Figure 14. High- z quasar candidates in the VIKING Z, Y, J colour plane. The dashed line shows the benchmark colour selection region. Grey circles show all VIKING candidates falling within this region after applying the benchmark morphological and photometric constraints described in the main text. A fraction of these objects are high priority candidates awaiting follow-up but most were rejected as result of probabilistic ranking or due to optical associations with SDSS sources. Crosses and open circles are candidates observed in I_{NTT} and Z_{NTT} . Open circles were undetected in I_{NTT} and have I_{NTT} , Z_{NTT} , Y, J colours consistent with $6.5 \leq z \leq 7.0$ quasars. Error bars show 1σ uncertainties.

350 deg^2 of data available at the time. To conduct a full and rigorous search of this data set a selection strategy was required in advance of the availability of most science ready data products. This made it difficult to develop a robust set of quasar selection constraints which optimise both efficiency in photometric and spectroscopic follow-up, whilst simultaneously selecting a highly complete sample of quasars.

To remedy this, we have modelled the cool star component of the VIKING catalogue in the Z, Y, J passbands to mimic contamination of quasar colour space by dwarf stars of spectral type M, L and T. We have compared this model to $\sim 1 \text{ deg}^2$ of imaging in the VIKING-VIDEO-CFHTLS overlap region using photometry from the complementary g, i, J, Ks colours as a robust star-galaxy separator. The model and data are in good agreement and we use it along with a sample of galaxies from the same overlapping data set to place constraints on the photometric and morphological characteristics of quasar colour space contaminants. This allows us to define a set of benchmark photometric and morphological selection cuts which will limit follow-up candidates to ~ 1 object per 3 deg^2 , an initial requirement of the follow-up campaign. The completeness of this search strategy is comparable to similar quasar searches conducted both in the optical and the near-IR.

Follow-up imaging of the first quasar candidates from

the NTT provides considerable support for the choice of benchmark constraints. Of 44 candidates observed in either I_{NTT} or both I_{NTT} and Z_{NTT} , just 5 have colours consistent with $6.5 \leq z \leq 7.5$ quasars. All 5 of these sources have VIKING colours that place them within our benchmark selection constraints.

Several other optical and near-IR surveys are due to either see their first light or to release their first products in the near future (e.g. Pan-STARRS, VST-KIDS, VHS). The tendency with large surveys is to place priority initially on the timely release of a small volume of data from a few well studied fields (VIKING being no exception). The methodology described here will provide an equally complementary set of methods with which to assess the first data from these forthcoming catalogues, allowing benchmark constraints to be placed on all rare object searches.

As surveys and corresponding data volumes begin to enter the Peta-byte era, rare object searches employing simple colour cuts are becoming cumbersome and inefficient. Several authors have already begun to prioritise follow-up candidates by combining observables to place them in a well defined ranking scheme (Richards et al. 2009; Yèche et al. 2010; Bovy et al. 2011). The first such ranking algorithm for high- z quasar candidates, uses Bayesian model comparison techniques to determine the probability that a given source has scattered from the quasar locus (Mortlock et al. 2011). In principle this methodology does away with colour cuts all together retaining and treating information that is normally lost or considered qualitatively, in a robust mathematical framework. The algorithm presented by Mortlock et al. requires accurate models of the photometry of cool stars and quasars specific to the particular survey it is applied to. Ideally the stellar model is constrained via maximum likelihood fits to the real data. In the case of VIKING and several other surveys this is not possible with the limited data expected from initial releases.

In a forthcoming paper we will present quasar candidates selected from the VSA by applying the stellar model developed here to the Mortlock et al. algorithm. We will discuss the success of this approach to modelling the stellar population by characterising a sample of test set data. We will also discuss in detail, the techniques necessary for defining the input catalogue from VSA archived photometry. Our hope is that this will provide a starting point from which to encourage future independent quasar searches in the VIKING data. This shows the diversity of the tools developed here in the context of high- z quasar and other rare object searches.

8 ACKNOWLEDGEMENTS

The authors would like to thank Jim Emerson and Karim Malik for their support and helpful discussion. We would also like to thank the UK team responsible for the realisation of VISTA, and the ESO team who operate and maintain this new facility. The UK's VISTA Data Flow System comprising the VISTA pipeline at the Cambridge Astronomy Survey Unit (CASU) and the VISTA Science Archive at the Wide Field Astronomy Unit (Edinburgh) (WFAU) provided calibrated data products and is supported by STFC.

The Besançon Simulations have been executed on com-

puters from the Utinam Institute of the Université de Franche-Comté, supported by the Région de Franche-Comté and Institut des Sciences de l'Univers (INSU)

We also make use of data based on observations obtained with MegaPrime/MegaCam, a joint project of CFHT and CEA/DAPNIA, at the Canada-France-Hawaii Telescope (CFHT) which is operated by the National Research Council (NRC) of Canada, the Institut National des Science de l'Univers of the Centre National de la Recherche Scientifique (CNRS) of France, and the University of Hawaii. This work is based in part on data products produced at TERAPIX and the Canadian Astronomy Data Centre as part of the Canada-France-Hawaii Telescope Legacy Survey, a collaborative project of NRC and CNRS.

REFERENCES

- Allard F., Hauschildt P. H., Alexander D. R., Starrfield S., 1997, *ARA&A*, 35, 137
- Barger A. J., Cowie L. L., Mushotzky R. F., Yang Y., Wang W., Steffen A. T., Capak P., 2005, *AJ*, 129, 578
- Bochanski J. J., Hawley S. L., Covey K. R., West A. A., Reid I. N., Golimowski D. A., Ivezić Ž., 2010, *AJ*, 139, 2679
- Bovy J., Hennawi J. F., Hogg D. W., et al., 2011, *ApJ*, 729, 141
- Boyle B. J., Shanks T., Croom S. M., Smith R. J., Miller L., Loaring N., Heymans C., 2000, *MNRAS*, 317, 1014
- Burningham B., Pinfield D. J., Lucas P. W., et al., 2010, *MNRAS*, 406, 1885
- Caballero J. A., Burgasser A. J., Klement R., 2008, *A&A*, 488, 181
- Chen B., Stoughton C., Smith J. A., et al., 2001, *ApJ*, 553, 184
- Cowie L. L., Songaila A., Hu E. M., Cohen J. G., 1996, *AJ*, 112, 839
- Croom S. M., Richards G. T., Shanks T., et al., 2009, *MNRAS*, 399, 1755
- Emerson J. P., Irwin M. J., Lewis J., et al., 2004, in P. J. Quinn & A. Bridger ed., *Society of Photo-Optical Instrumentation Engineers (SPIE) Conference Series Vol. 5493 of Society of Photo-Optical Instrumentation Engineers (SPIE) Conference Series*, VISTA data flow system: overview. pp 401–410
- Emerson J., Sutherland W., 2010, *The Messenger*, 139, 2
- Fan X., 1999, *AJ*, 117, 2528
- Fan X., Narayanan V. K., Lupton R. H., et al., 2001, *AJ*, 122, 2833
- Fan X., Strauss M. A., Schneider D. P., et al., 2003, *AJ*, 125, 1649
- Fan X., Strauss M. A., Becker R. H., et al., 2006, *AJ*, 132, 117
- Francis P. J., Hewett P. C., Foltz C. B., Chaffee F. H., Weymann R. J., Morris S. L., 1991, *ApJ*, 373, 465
- Glikman E., Djorgovski S. G., Stern D., Dey A., Jannuzi B. T., Lee K., 2011, *ApJL*, 728, L26
- Gunn J. E., Stryker L. L., 1983, *ApJS*, 52, 121
- Hambly N. C., Mann R. G., Bond I., Sutorius E., Read M., Williams P., Lawrence A., Emerson J. P., 2004, in P. J. Quinn & A. Bridger ed., *Society of Photo-Optical Instrumentation Engineers (SPIE) Conference Series Vol. 5493 of Society of Photo-Optical Instrumentation Engineers (SPIE) Conference Series*, VISTA data flow system survey access and curation: the WFCAM science archive. pp 423–431
- Haywood M., Robin A. C., Creze M., 1997, *A&A*, 320, 440
- Hewett P. C., Foltz C. B., Chaffee F. H., 1995, *AJ*, 109, 1498
- Hewett P. C., Warren S. J., Leggett S. K., Hodgkin S. T., 2006, *MNRAS*, 367, 454
- Hodgkin S. T., Irwin M. J., Hewett P. C., Warren S. J., 2009, *MNRAS*, 394, 675

- Irwin M. J., Lewis J., Hodgkin S., et al., 2004, in P. J. Quinn & A. Bridger ed., *Society of Photo-Optical Instrumentation Engineers (SPIE) Conference Series Vol. 5493 of Society of Photo-Optical Instrumentation Engineers (SPIE) Conference Series*, VISTA data flow system: pipeline processing for WFCAM and VISTA. pp 411–422
- Jiang L., Fan X., Vestergaard M., Kurk J. D., Walter F., Kelly B. C., Strauss M. A., 2007, *AJ*, 134, 1150
- Jiang L., Fan X., Annis J., et al., 2008, *AJ*, 135, 1057
- Jiang L., Fan X., Brandt W. N., Carilli C. L., Egami E., Hines D. C., Kurk J. D., Richards G. T., et al., 2010, *Nature*, 464, 380
- Juarez Y., Maiolino R., Mujica R., Pedani M., Marinoni S., Nagao T., Marconi A., Oliva E., 2009, *A&A*, 494, L25
- Jurić M., Ivezić Ž., Brooks A., et al., 2008, *ApJ*, 673, 864
- Kaiser N., et al., 2002, in J. A. Tyson & S. Wolff eds., *Society of Photo-Optical Instrumentation Engineers (SPIE) Conference Series Vol. 4836 of Society of Photo-Optical Instrumentation Engineers (SPIE) Conference Series*, Pan-STARRS: A Large Synoptic Survey Telescope Array. p. 154
- Kirkpatrick J. D., 2005, *ARA&A*, 43, 195
- Komatsu E., Dunkley J., Nolte M. R., et al., 2009, *ApJS*, 180, 330
- Lawrence A., et al., 2007, *MNRAS*, 379, 1599
- Leggett S. K., Burningham B., Saumon D., et al., 2010, *ApJ*, 710, 1627
- Lejeune T., Cuisinier F., Buser R., 1997, *A&AS*, 125, 229
- Lodieu N., Burningham B., Hambly N. C., Pinfield D. J., 2009, *MNRAS*, 397, 258
- Lupton R. H., Gunn J. E., Szalay A. S., 1999, *AJ*, 118, 1406
- Maddox N., Hewett P. C., Warren S. J., Croom S. M., 2008, *MNRAS*, 386, 1605
- Maiolino R., 2009, in Giobbi G., Tornambe A., Raimondo G., Limongi M., Antonelli L. A., Menci N. & Brocato E., eds, Vol. 1111 of *American Institute of Physics Conference Series*, Early metal enrichment in high-redshift quasars. AIP, Melville, New York. p. 160
- Mortlock D. J., Patel M., Warren S. J., et al., 2009, *A&A*, 505, 97
- Mortlock D. J., Patel M., Warren S. J., Hewett P. C., Venemans B. P., McMahon R. G., Simpson C. J., 2011, *ArXiv e-prints*
- Mortlock D. J., Warren S. J., Venemans B. P., et al. 2011, *Nature*, 474, 616
- Patel M., 2010, PhD thesis, Imperial College London
- Richards G. T., Fan X., Newberg H. J., et al., 2002, *AJ*, 123, 2945
- Richards G. T., Strauss M. A., Fan X., et al., 2006, *AJ*, 131, 2766
- Richards G. T., Deo R. P., Lacy M., et al., 2009, *AJ*, 137, 3884
- Robin A. C., Reylé C., 2003, in J. M. De Buizer & N. S. van der Blied ed., *Galactic Star Formation Across the Stellar Mass Spectrum Vol. 287 of Astronomical Society of the Pacific Conference Series*, The Initial Mass Function at Low Masses. pp 104–109
- Robin A. C., Reylé C., Derrière S., Picaud S., 2003, *A&A*, 409, 523
- Rowan-Robinson M., Babbedge T., Oliver S., et al., 2008, *MNRAS*, 386, 697
- Schmidt M., Schneider D. P., Gunn J. E., 1995, *AJ*, 110, 68
- Schneider D. P., Hall P. B., Richards G. T., et al., 2007, *AJ*, 134, 102
- Schultheis M., Robin A. C., Reylé C., McCracken H. J., Bertin E., Mellier Y., Le Fèvre O., 2006, *A&A*, 447, 185
- Shen Y., Strauss M. A., Oguri M., et al., 2007, *AJ*, 133, 2222
- Skrutskie M. F., Cutri R. M., Stiening R., et al., 2006, *AJ*, 131, 1163
- Stiavelli M., Djorgovski S. G., Pavlovsky C., et al., 2005, *ApJL*, 622, L1
- Venemans B. P., McMahon R. G., Warren S. J., Gonzalez-Solares E. A., Hewett P. C., Mortlock D. J., Dye S., Sharp R. G., 2007, *MNRAS*, 376, L76
- Warren S., Hewett P., 2002, in Metcalfe N., Shanks T., eds, *A New Era in Cosmology Vol. 283 of Astronomical Society of the Pacific Conference Series*, WFCAM, UKIDSS, and $z = 7$ Quasars. p. 369
- Wiese W. L., Smith M. W., Glennon B. M., 1966, *NSRDS-NBS 4*, Atomic Transition Probabilities. Vol. I: Hydrogen through Neon. A Critical Data Compilation. US Department of Commerce, National Bureau of Standards, Washington, DC
- Willott C. J., Percival W. J., McLure R. J., Crampton D., Hutchings J. B., Jarvis M. J., Sawicki M., Simard L., 2005, *ApJ*, 626, 657
- Willott C. J., Delfosse X., Forveille T., Delorme P., Gwyn S. D. J., 2005, *ApJ*, 633, 630
- Willott C. J., Delorme P., Reylé C., et al., 2010, *AJ*, 139, 906
- Yèche C., Petitjean P., Rich J., et al., 2010, *A&A*, 523, A14
- York D. G., Adelman J., Anderson Jr. J. E., et al., 2000, *AJ*, 120, 1579
- Zhang Z. H., Pokorný R. S., Jones H. R. A., et al., 2009, *A&A*, 497, 619